JOURNAL OF CATALYSIS **176,** 513–526 (1998)
ARTICLE NO. CA982071

On the Unusually High Apparent Activation Energy of Chemical Conversion under Single-File Conditions

Christian Rödenbeck, Jörg Kärger,[1] and Karsten Hahn

Universität Leipzig, Fakultät für Physik und Geowissenschaften, Linnéstrasse 5, D-04103 Leipzig, Germany

Received November 13, 1997; revised March 2, 1998; accepted March 2, 1998

The temperature behaviour of transport-reaction systems undergoing single-file diffusion (the particles are not able to change their order) is investigated systematically. The influence of exchange limitations at the margins, of attraction between the particles, and of a small possibility that adjacent particles exchange their positions are considered. The investigation is based on an isoline diagram which proves to be a very useful tool applicable to any transport-reaction system. If the channels are crowded, if the intrinsic reaction rate is large enough so that the total conversion is transport-controlled, and if the activation energies of the elementary processes of the transport fulfil certain relations (e.g., if passages of neighbouring particles are possible with an activation energy higher than the intrinsic activation energy of the conversion), then the apparent activation energy of the conversion in the single-file system can exceed the intrinsic activation energy. Such a behaviour is impossible for systems undergoing normal diffusion but was found experimentally for some single-file zeolites in the literature.

1. INTRODUCTION

Chemical conversion with zeolitic catalysts whose transport dynamics follows the laws of single-file diffusion have recently been the subject of quite a number of both experimental and theorectical studies (1–9). Single-file diffusion occurs in zeolites with a one-dimensional pore structure as soon as the guest molecules are too large to be able to pass each other within the channels (8, 9). This causes a considerable mutual hindrance of the mobility of the molecules, giving rise to various unusual phenomena.

When Sachtler *et al.* investigated the temperature dependence of chemical conversions in zeolitic catalysts where the molecular transport can be expected to exhibit single-file behaviour, they found that the apparent activation energy of the total output of these single-file catalysts *exceeded* the activation energy of the intrinsic reaction rate (1–3). This is a surprising result since, within the realm of normal diffusion, any transport limitation surely *reduces* this apparent activation energy. It is even more striking if one keeps in mind that the transport limitation due to single-file diffusion is far more serious than that due to normal diffusion. However, they were able to give a qualitative argument, indicating that the observed behaviour could in fact be the *consequence* of the single-file restriction (3): The reduction of the apparent activation energy in the case of normal diffusion is caused by the fact that, with increasing temperature, the catalyst gets depopulated. However, in a single-file system the mobility of the individual particles depends (much more pronouncedly than in the case of normal diffusion) on the particle concentration. Hence, if the temperature is raised, the mobility of the particles increases dramatically as a consequence of the decreasing density. A higher mobility, in turn, leads to a higher effectiveness of the conversion. This effect may eventually overcompensate for the loss of total particle number. As the result, the total output of the single-file catalyst increases more quickly than the intrinsic conversion.

In order to assess this argumentation in a more quantitative way, Monte Carlo simulations were carried out (5). The single-file diffusion was modelled by an activated jump mechanism on discrete adsorption sites where double occupancy was forbidden. It turned out that an unusual activation energy as described above can indeed occur. Nevertheless, the values of the adsorption energy which had to be assumed in this study are not very realistic for zeolites.

The present paper investigates a more sophisticated model of the single-file system than that used for the simulations of Ref. (5). Further types of interactions which can be expected to occur in real zeolitic systems are included into this model. The aim of our investigation was to study systematically the influence of these interactions on the temperature behaviour of the chemical reaction. Special emphasis was given to the occurrence of an *apparent activation energy exceeding the true activation energy*, and to the question which of the interactions intensify (or reduce, respectively) this enhancement of the apparent activation energy. The paper clearly concentrates on the basic features of single-file systems, rather than the far more complicated situation in real zeolite structures. Although, therefore, the results cannot be compared quantitatively with the

[1] Corresponding author.

0021-9517/98 $25.00

observations of particular experiments, they suggest that single-file restriction may well cause effects like those described above.

A procedure able to tackle the posed problem is developed in (6). This procedure yields the concentrations and the effectiveness factors for a quite general model of the single-file system by numerical solution of a set of linear equations. It allows a larger parameter range to be studied than by the simulations. The numerical results are represented by suitable isoline diagrams (5) which then allow a systematic discussion of the temperature behaviour of single-file catalysts.

The underlying model is presented in Section 2, introducing both the parameters (input quantities) and the quantities to be calculated in order to discuss the temperature behaviour (output quantities). Section 3 describes in detail the isoline diagram as the powerful tool used for the discussion of this paper. It explains how information can be drawn from this diagram both qualitatively and quantitatively. Employing these methods, Section 4 investigates the temperature dependence of the conversion under single-file conditions for several cases. Conditions are given under which the apparent activation energy E_{app} exceeds the intrinsic activation energy E_{true} of the conversion. The Appendix gives some remarks concerning the generalizations that had to be made to the algorithm of (6) in order to suit the present model.

2. THE MODEL

2.1. Input Quantities

The investigation is based on a discrete model of the single-file system. It is a generalization of that already used in (6). The single-file channel is considered as a linear chain of N adsorption sites, formed by potential troughs as shown schematically in Fig. 1. An isolated particle (i.e., in the absence of interactions with other particles) hops from intracrystalline sites to adjacent ones with a rate Γ, leading to a single-particle diffusion coefficient

$$D = l^2 \cdot \Gamma \qquad [1]$$

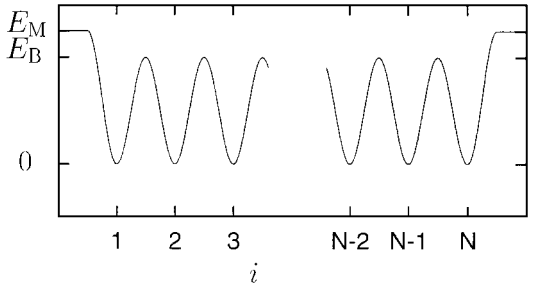

FIG. 1. Profile of the channel–particle interaction potential (schematically). The abscissa i represents the number of the site.

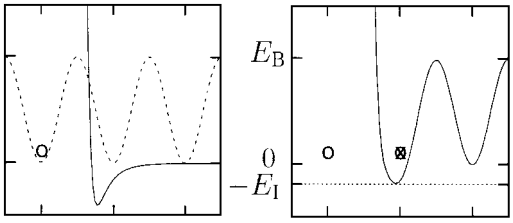

FIG. 2. Particle–particle interaction potential caused by the particle ○ (left-hand side) and resulting total potential felt by particle ⊗ (right-hand side).

if the sites are separated by the distance l. If the isolated particle occupies one of the marginal sites it jumps out of the channel into the surrounding gas phase with the rate ε. A particle from outside jumps onto one of the marginal sites with the rate α.

The particle–particle interactions are assumed as follows. As indicated on the left-hand side of Fig. 2, a particle (symbolized by "○") causes an additional potential which is repulsive at very short distances but attractive at larger distances. On the right-hand side, the total potential as felt by the neighboring particle (symbolized by "⊗") is given. In contrast to an isolated particle, the particle "⊗" is not able to jump to the site already occupied by the particle "○." This causes single-file behaviour because it forces the particles to maintain their order within the channel. Further, if the particle "⊗" tries to jump away from the particle "○," it has to surmount an increased potential barrier, whence the hop rate is reduced from Γ to $\omega\Gamma$ with the interaction parameter $\omega \leq 1$.

Up to now, the model represents a single-file system in the strict sense, where any possibility that particles change their order is excluded. Additionally, we assume that mutual passages of particles located at adjacent sites can occur with the rate $\xi\Gamma$ (the particles exchange their positions).

Eventually, there is the chemical reaction, taking place at the catalytically active adsorption sites. All particles coming from the gas phase shall exclusively be reactant molecules. Within the channel, they are converted into product molecules by a monomolecular irreversible reaction with the intrinsic rate k. The transport properties of both reactant and product molecules are assumed to be identical, and there shall be no statistical dependence between the conversion and the hops.

All the processes described so far are activated, so that we may assume Arrhenius laws for all the rates

$$\Gamma = \hat{\Gamma} e^{-E_B/RT} \qquad [2]$$

$$\alpha = \hat{\alpha} \qquad [3]$$

$$\varepsilon = \hat{\varepsilon} e^{-E_M/RT} \qquad [4]$$

$$\omega\Gamma = \hat{\Gamma} e^{-(E_B+E_I)/RT} \qquad [5]$$

$$\xi\Gamma = \hat{\xi}\hat{\Gamma}e^{-E_X/RT} \quad [6]$$

$$k = \hat{k}e^{-E_{true}/RT} \quad [7]$$

with E_B denoting the potential barrier between adjacent sorption sites (cf. Fig. 1); E_M, the potential barrier to be surmounted by desorbing particles (sorption heat); E_I, the interaction energy by which a site adjacent to an occupied site is "deeper" (cf. Fig. 2); E_X, the potential barrier for passages; E_{true}, the activation energy of the intrinsic reaction; and RT, the thermal energy at the temperature T. The number of parameters can be reduced by introducing dimensionless parameters, replacing the rates α, ε, k, and Γ:

$$v := \frac{\varepsilon}{\alpha}, \quad [8]$$

$$a := \frac{\alpha}{2\Gamma}, \quad [9]$$

$$\kappa := \frac{k}{2\Gamma}. \quad [10]$$

(These definitions are consistent to (5, 6).) Now the mean time between successive hop attempts of the particles, $1/2\Gamma$, simply plays the part of the time unit. The following set of parameters (all of which fulfil Arrhenius laws, too) represent the input quantities of our model:

$$v = \hat{v}e^{-E_v/RT} \quad \text{with } \hat{v} = \hat{\varepsilon}/\hat{\alpha};\ E_v = E_M. \quad [11]$$

This parameter v, representing the ratio between the desorption and adsorption rates, controls (in connection with the parameter ω) the overall coverage Θ (relative amount of occupied sites), where, owing to its definition, small values of v correspond to large values of Θ and vice versa. (A representation showing the relation between Θ and v shall be found in Fig. 6.)

$$\kappa = \hat{\kappa}e^{-E_\kappa/RT} \quad \text{with } \hat{\kappa} = \hat{k}/2\hat{\Gamma};\ E_\kappa = E_{true} - E_B. \quad [12]$$

This parameter κ simply gives the intrinsic conversion rate in terms of the time unit $1/2\Gamma$:

$$a = \hat{a}e^{-E_a/RT} \quad \text{with } \hat{a} = \hat{\alpha}/2\hat{\Gamma};\ E_a = -E_B. \quad [13]$$

This parameter a gives, similar to κ, the adsorption rate in terms of the time unit $1/2\Gamma$. This parameter will be used to characterize the particle exchange between the marginal sites of the channel and the surrounding gas phase:

$$\omega = \hat{\omega}e^{-E_\omega/RT} \quad \text{with } \hat{\omega} = 1,\ E_\omega = E_I. \quad [14]$$

This parameter ω controls the attractive interaction of adjacent particles. If $\omega = 1$ there is no attraction:

$$\xi = \hat{\xi}e^{-E_\xi/RT} \quad \text{with } E_\xi = E_X - E_B. \quad [15]$$

This parameter ξ characterizes the deviation of the system from the strict single-file condition: While the ideal single-file system implies $\xi = 0$, an increasing ξ means an increasing rate of site exchanges (passages) between adjacent molecules.

2.2. Example Values

Of course, the transport mechanisms in real zeolites are much more complicated than that of our jump model. Nevertheless, we give some example values of the parameters, providing an idea of realistic orders of magnitude. Unfortunately, there are, up to now, only few measurements of single-file behaviour reported in the literature.

At first, consider literature values of the activation energies. For neopentane in Pt/H-mordenite investigated in (3), an adsorption energy (E_M) around 50 kJ/mol was found. Activation energies of conversions (E_{true}) were reported between 105 kJ/mol (neopentane skeletal conversion over supported Pt in (3)) and around 200 kJ/mol (neopentane conversion over supported Pd in (2)). Conclusive experimental data of the activation energy E_X of passages could not be found in the literature, but one might assume rather high values because the passing molecules have to come quite close within the narrow pores of single-file zeolites. MD simulations (12) gave potential barriers (E_B) for small organic molecules in $AlPO_4$-5 between 3 and 4 kJ/mol. This is much less than all the aforementioned values.

The rates can be estimated as follows. Reaction rates k are reported in (2) around $k \approx 10^{-4}$ s^{-1} at about 500 K. Intracrystalline single-particle diffusivities of tetraflouromethane in $AlPO_4$-5 were reported to be around 10^{-6} m^2 s^{-1} (8, 9). This gives, via Eq. [1] with $l = 7$ Å for $AlPO_4$-5, $\Gamma \approx 10^{12}$ s^{-1}. Assuming that the jumps from the marginal sites out of the channel are activated by the same mechanism as the intracrystalline hops, one has at 500 K the ratio $\varepsilon/\Gamma = \exp(-[E_M - E_B]/RT) \approx 10^{-4}$. This gives $\varepsilon \approx 10^8$ s^{-1}. If we assume an interaction energy E_I of about 40 kJ/mol, one has an interaction parameter of $\omega \approx 10^{-4}$ at 500 K. The rate α of adsorption events from the gas phase might be identified with the number per time of collisions of gas molecules with an area of the size of the channel openings. This can be calculated by the formula of gas kinetics (10),

$$\alpha = \frac{p}{\sqrt{2\pi mkT}}A. \quad [16]$$

At atmospheric pressure, $p \approx 10^5$ Pa, and 500 K, one gets for methane ($m \cdot N_A = 16$ g/mol) and $AlPO_4$-5 ($A \approx 1.7 \times 10^{-18}$ m^2) the estimate $\alpha \approx 10^9$ s^{-1}. Example value for the dimensionless parameters therefore could be $v = \varepsilon/\alpha \approx 10^{-1}$ and $a = \alpha/2\Gamma \approx 10^{-3}$.

We stress, however, that the results of this paper will not be restricted to the special values given here but, corresponding to the aim of the paper, that we will consider the

behaviour of the model over a range of parameter values as wide as possible in order to get a comprehensive survey about its features.

2.3. Output Quantities

The total rate of product molecules put out by the catalyst in the equilibrium of the monomolecular irreversible reaction be K. Obviously, it can be related via

$$K = \mathrm{H}^* \cdot k \qquad [17]$$

to the intrinsic conversion rate k and the mean number H^* of reactant molecules in the catalysts. Assuming Arrhenius laws for K and H^* as well,

$$K = \hat{K} e^{-E_{\mathrm{app}}/RT}, \qquad [18]$$

$$\mathrm{H}^* = \hat{\mathrm{H}}^* e^{-E_{\mathrm{H}^*}/RT}, \qquad [19]$$

the *apparent activation energy* E_{app} of the total output is given by

$$E_{\mathrm{app}} = E_{\mathrm{H}^*} + E_{\mathrm{true}}. \qquad [20]$$

As mentioned in the Introduction, in Fickian diffusion-reaction systems one always has $E_{\mathrm{app}} < E_{\mathrm{true}}$, implying $E_{\mathrm{H}^*} < 0$. In this paper, however, we will be interested in the unusual case $E_{\mathrm{app}} > E_{\mathrm{true}}$ which can be expressed equivalently by the condition $E_{\mathrm{H}^*} > 0$.

Thus, the mean number H^* of reactant molecules is the relevant quantity on investigating the problem posed in the Introduction. This quantity is related to the effectiveness factor η and the relative concentration (coverage, occupation) Θ by (5)

$$\mathrm{H}^* = \Theta N \eta. \qquad [21]$$

3. THE ISOLINE REPRESENTATION

3.1. Qualitative Consideration

If one would intend to study the temperature dependence of the system as a function of the prefactors and the activation energies of all the parameters according to Eqs. [11] to [12], one were confronted with a much too large number of adjustable quantities. Therefore, in (5) a quite close representation of the system behaviour was introduced which allows the temperature dependence to be discussed in a very illustrative and systematic manner. This *isoline representation* was again used in (6). This paper discusses the properties and the benefit of this method in more detail.

As is seen from the estimates in Section 2.2, in zeolitic single-file systems the parameters κ and v (and, if passages are considered, ξ) possess the highest activation energies, thus showing the strongest temperature dependence. Thus, it would be instructive to know the dependence of the quantity H^* on κ and v at fixed values of the other parameters. A 3D plot like the example Fig. 3 would provide this information. Although this plot is illustrative, it does not suit a quantitative analysis. Figure 4 shows the isoline representation for the same set of parameters. The diagram spans the plane of the parameters κ and v. On moving over this plane in a vertical direction, the intrinsic rate of conversion changes, while the transport properties of the system remain the same. Along horizontal lines, on the contrary, the concentration and, thus, the transport behaviour changes, while the intrinsic conversion is fixed. Sloppily speaking, κ thus provides the "reaction axis" and v, the "transport axis." Within this (κ, v)-plane, the isolines connect all points with equal values of H^*. Like in geographic maps, "steep areas" (where H^* varies strongly with the parameters) have a high density of isolines and vice versa. The gradient giving the direction of the main influence is directed normal to the isolines.

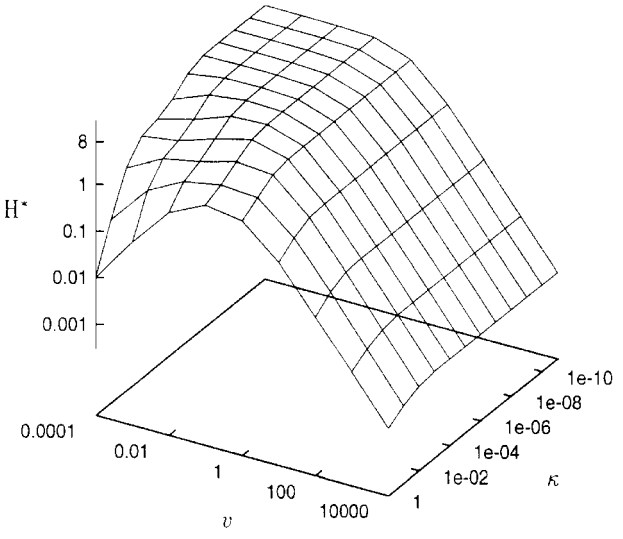

FIG. 3. Mean number H^* of reactant molecules within the channel in dependence on the intrinsic reaction rate κ (in units of the intracrystalline hop time $1/2\Gamma$) and the ratio v of desorption and adsorption rates. The presented behaviour is valid for the case of a rapid particle exchange between the marginal sites and the gas phase ($a = 50$), the absence of an attraction between the particles ($\omega = 1$), and a strict single-file system where passages are inhibited ($\xi = 0$). The data of this representation (as well as those of the following figures) have been calculated by the method described in Appendix A. Since single-file systems of eight sites have been considered, the maximum value of H^* is equal to 8.

Now, how can the temperature behaviour be read from this diagram? If E_κ, $\hat{\kappa}$, E_v, and $\hat{v}$ are fixed, both $(\ln \kappa)$ and $(\ln v)$ are proportional to $(1/RT)$. Thus, since the isoline diagram has log axes, varying the temperature means moving on a straight line in the (κ, v)-plane. Figure 4 shows two examples of such a "temperature line" for special, fictive values of the afore-mentioned quantities as broken lines. The direction of the temperature line is determined by the ratio E_κ / E_v, while the prefactors $\hat{\kappa}$ and $\hat{v}$ translate the line. A section of the H^*-landscape along this temperature line is nothing else than the Arrhenius plot $(\ln \mathrm{H}^*)$ versus $(1/RT)$,

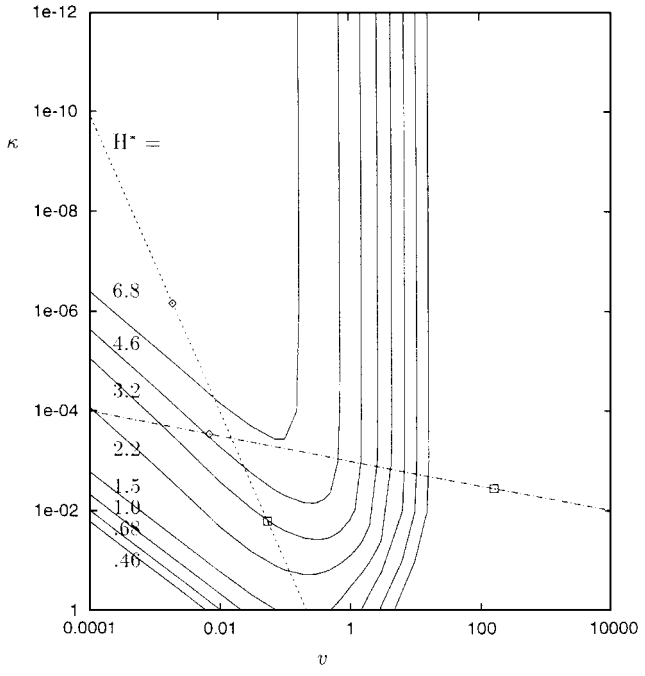

FIG. 4. The same information as in Fig. 3, presented as isolines of H* over the plane of the parameters κ and υ. (Here and in all the following isoline diagrams, the isolines refer to reactant particle numbers 6.8, 4.6, ... down to 0.46.) Since the parameters κ and υ are temperature dependent, a variation of the temperature corresponds to a displacement in the parameter plane along a straight line, two examples of which are indicated by the broken lines (- - - -: $E_\kappa = 150$ kJ/mol, $\hat{\kappa} = 10^{20}$, $E_\upsilon = 50$ kJ/mol, $\hat{\upsilon} = 10^6$; -·-·-·- : $E_\kappa = 37.5$ kJ/mol, $\hat{\kappa} = 10^3$, $E_\upsilon = 150$ kJ/mol, $\hat{\upsilon} = 10^{24}$). Each of these "temperature lines" wears two labels, corresponding to the temperatures 300 K (◇) and 360 K (□), respectively.

valid for the chosen temperature dependence of the parameters κ and υ. The more isolines are crossed by a fixed part of the temperature line, the stronger, H* depends on temperature, i.e., the larger is the absolute value of E_{H^*}. If one crosses the isolines with the increasing temperature in ascending order, then E_{H^*} is positive and vice versa. Thus, one can read from Fig. 4 for one of the examples shown there (-·-·-·-) that E_{H^*} is positive for values of υ smaller than roughly 0.1 and negative for υ larger than roughly 0.1. (Qualitatively, this resembles, according to Eq. [20], the break in the Arrhenius plot of K found experimentally in (3). The possibility of positive values of E_{H^*} confirms that the apparent activation energy E_{app} of the total conversion may exceed the true activation energy E_{true} of the conversion.)

Summing up, the situation is as follows. On the one hand, the isoline diagram reflects the complete information about the system behaviour at fixed values of the parameters a, ω, and ξ. On the other hand, the direction and position of the temperature line contain all information about the temperature dependence of the parameters κ and υ. If these two parameters are the only temperature-dependent ones, a complete overview about the temperature behaviour of the system can be obtained in a very illustrative way by rotating and translating the temperature line over the (κ, υ)-plane and assessing the values of E_{H^*} in each case. Section 3.2 will give a quantitative procedure to do this. If the temperature dependence of one of the other parameters, a, ω, or ξ, cannot be neglected, one has to consider several isoline diagrams belonging to different values of the respective parameter. This procedure, too, will be explained in Section 3.2 and exemplified in Section 4.

The causes generating the actual topology of Figs. 3 and 4 become obvious in Fig. 5, where the isolines of the concentration Θ and the effectiveness factor η, which constitute H* via Eq. [21], are represented separately.

- The isolines of the *concentration* Θ are parallel to the κ-axis because the concentration does not depend on κ. Every section parallel to the υ-axis leads to the function $\Theta = \Theta(\upsilon)$, two examples of which are shown in Fig. 6 (above). For small υ, the concentration is approximately constant, whence there are no more isolines in this region, while the power-law decay at increasing υ leads to equidistant isolines.
- A section of the isoline representation of the *effectiveness factor* η parallel to the κ-axis yields the dependences $\eta = \eta(\kappa)$ shown in Fig. 7. At small κ, the reaction is chemically controlled ($\eta = 1$), while at large κ the influence of the transport processes becomes dominant, leading to a decrease of the effectiveness factor with increasing intrinsic rate.

The landscape of H* is an obvious combination of the landscapes of Θ and η. According to the respective behaviour of these two quantities, the (κ, υ)-parameter plane can be divided into four regions, summarized schematically in Fig. 8.

3.2. Quantitative Consideration

With the considerations of the previous section, we got a qualitative survey of the situation. In Ref. (5), the isoline representation was used to determine the activation energy E_{H^*} quantitatively by graphical means. Now, we extent this method in order to faciliate a general discussion.

If we consider H* as a function of the parameters υ, a, ω, ξ, and κ, the total differentiation of (ln H*) with respect to $(1/RT)$ gives

$$E_{H^*} = \frac{\partial \ln H^*}{\partial \ln \upsilon} E_\upsilon + \frac{\partial \ln H^*}{\partial \ln a} E_a + \frac{\partial \ln H^*}{\partial \ln \omega} E_\omega + \frac{\partial \ln H^*}{\partial \ln \xi} E_\xi + \frac{\partial \ln H^*}{\partial \ln \kappa} E_\kappa, \qquad [22]$$

where we made use of the Arrhenius laws. Now we try to relate the terms of this equation to the information provided by the isoline diagram.

At first, we consider the regions III and IV, where the effectiveness factor decreases with increasing intrinsic rate of conversion.

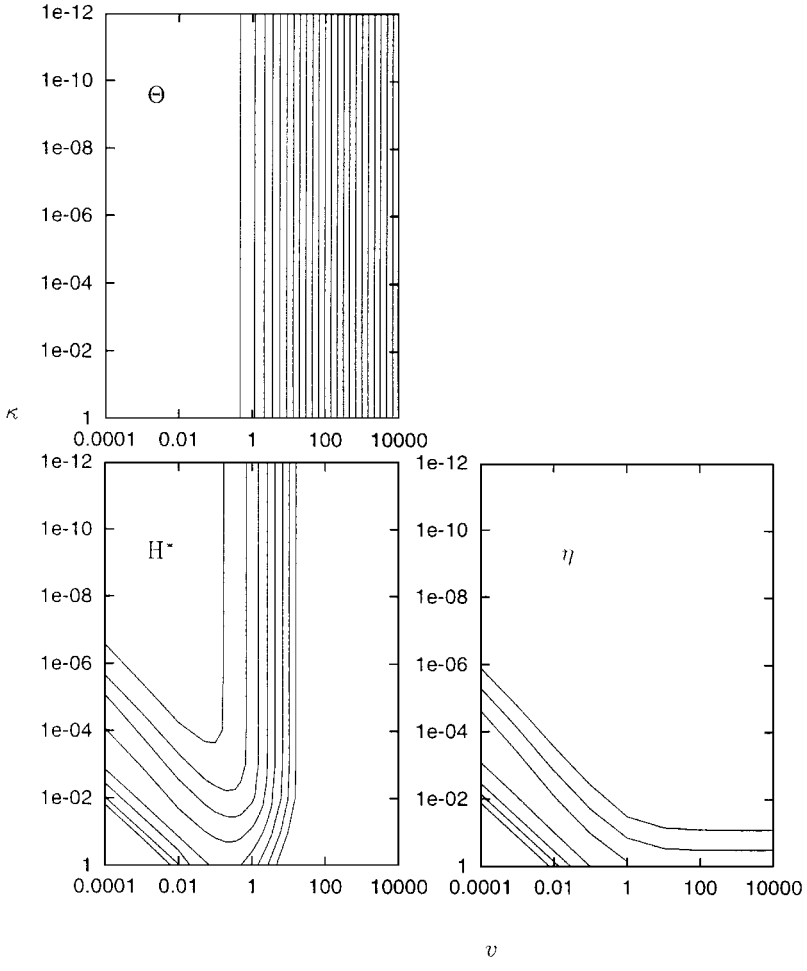

FIG. 5. Illustration of the origin of the topology as shown in Figs. 3 and 4. The "landscapes" of the concentration Θ and the effectiveness factor η combine according to the relation $H^* = \Theta N \eta$—Eq. [21]—yielding the "landscape" of the mean number of reactant molecules. (Again, all isolines for $H^* < 0.46$ are omitted.)

- In this region, the slope coefficient

$$B := -\frac{\partial \ln H^*}{\partial \ln \kappa} \qquad [23]$$

is sure to be positive. Obviously, it can be read in the isoline diagram from the *mutual distance of adjacent isolines*, measured on a line parallel to the κ-axis at the considered value of υ. We will, however, use an alternative way and calculate the coefficient B from the function $\eta = \eta(k)$ by

$$B = -\frac{\partial \ln \eta}{\partial \ln \kappa} = -\frac{E_{\text{true}}}{E_\kappa}\frac{\partial \ln \eta}{\partial \ln k} \qquad [24]$$

as follows from Eqs. [21] and [10].

- Further, we choose an arbitrary isoline and consider it as a function $\kappa = \kappa(\upsilon)$, implicitly defined by the condition ($\ln H^* = \text{const}$). From the total derivative of this condition with respect to ($\ln \upsilon$) one gets

$$\frac{\partial \ln H^*}{\partial \ln \kappa}\frac{d \ln \kappa}{d \ln \upsilon} + \frac{\partial \ln H^*}{\partial \ln \upsilon} = 0$$

because the other parameters, a, ω, and ξ, are, per definition, constant on the isoline. Obviously, the quantity

$$A_\upsilon := \frac{d \ln \kappa}{d \ln \upsilon} \qquad [25]$$

can be read from the diagram as the *angular coefficient of the isolines*.

- At last, we take a fixed value of υ and consider the corresponding point on the chosen isoline. If we now vary one of the other parameters, say a, this point will be translated parallel to the κ-axis because the isoline pattern changes. If we consider the κ-coordinate of the point as a function of this parameter a, again implicitly defined by the condition ($\ln H^* = \text{const}$), we get analogously

$$\frac{\partial \ln H^*}{\partial \ln \kappa}\frac{d \ln \kappa}{d \ln a} + \frac{\partial \ln H^*}{\partial \ln a} = 0.$$

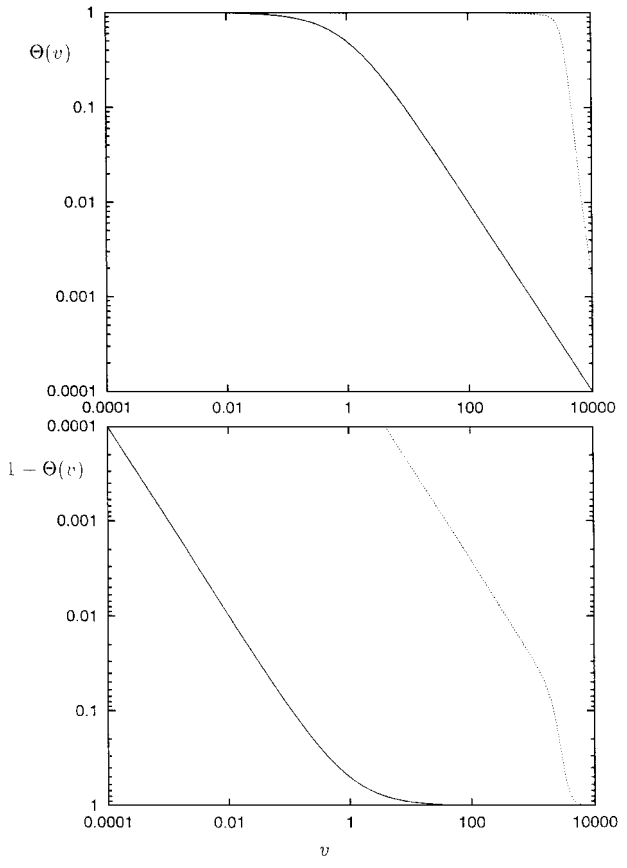

FIG. 6. Dependence of the concentration Θ (above) and the "vacancy concentration" $(1-\Theta)$ (below) on the parameter υ for $\omega = 1$ (no attraction, as assumed in most of the other figures, curve ———) or $\omega = 10^{-4}$ (strong attractive interaction between molecules at adjacent sites as assumed in Fig. 11, curve · · ·). The marginal exchange rate (parameter a) and the possibility of passages (parameter ξ) do not influence the concentration.

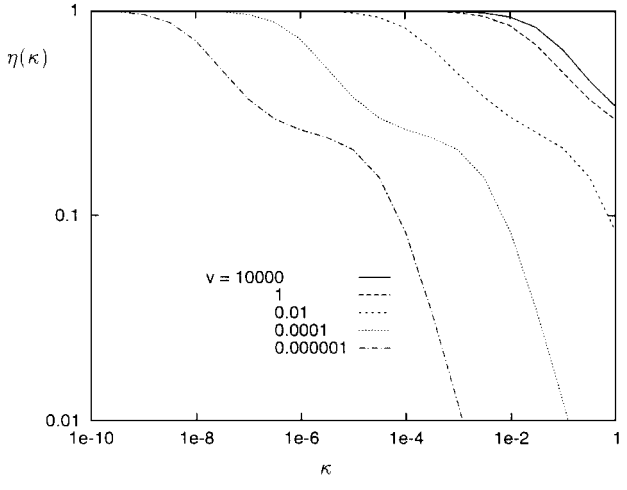

FIG. 7. Dependence of the effectiveness factor η on the parameter κ for different values of υ. Parameters a, ω, and ξ identical to the previous figures.

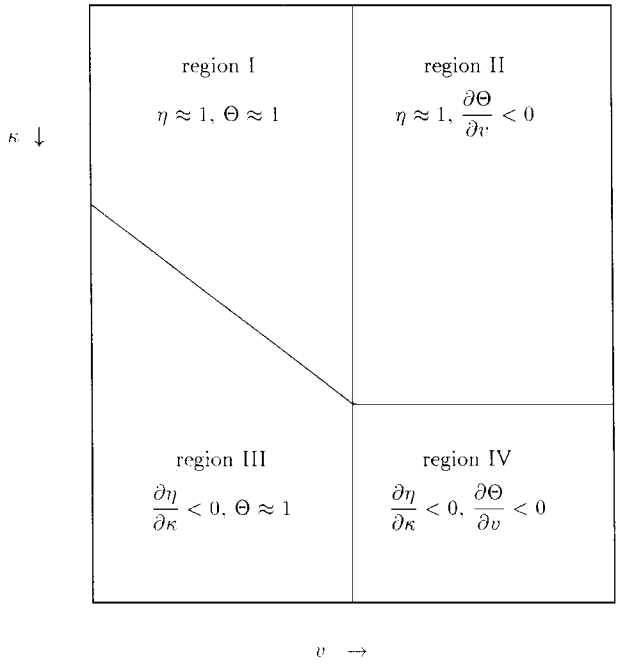

FIG. 8. Subdivision of the (κ, υ)-parameter plane into four regions according to the respective behaviour of the functions $\Theta = \Theta(\upsilon)$ and $\eta = \eta(\kappa)$ (schematically).

According to this calculation, the quantity

$$A_a := \frac{\mathrm{d}\ln\kappa}{\mathrm{d}\ln a} \qquad [26]$$

can be read from the *displacement of the isolines* on comparing isoline diagrams belonging to different values of a (but identical values of the other parameters). Analogous considerations are true for the parameters ω and ξ, involving the displacement coefficients

$$A_\omega := \frac{\mathrm{d}\ln\kappa}{\mathrm{d}\ln\omega}, \qquad [27]$$

$$A_\xi := \frac{\mathrm{d}\ln\kappa}{\mathrm{d}\ln\xi}. \qquad [28]$$

Introducing all these equations into Eq. [22] gives

$$E_{\mathrm{H}^*} = B(A_\upsilon E_\upsilon + A_a E_a + A_\omega E_\omega + A_\xi E_\xi - E_\kappa). \qquad [29]$$

Since $B > 0$, the criterion for E_{app} exceeding E_{true} reads

$$A_\upsilon E_\upsilon + A_a E_a + A_\omega E_\omega + A_\xi E_\xi > E_\kappa. \qquad [30]$$

In region I one has, according to Eq. [21], $\mathrm{H}^* = N$, independent of the temperature, whence $E^{\mathrm{I}}_{\mathrm{H}^*} = 0$. In region II, $\mathrm{H}^* = \Theta N$ depends only on the concentration (this corresponds to the fact that the isolines are parallel to the κ-axis) and decreases proportionally to Θ with increasing υ. A calculation analogous to that for regions III and IV

yields the formula:

$$E_{H^*}^{II} = B^{II}\left(A_\omega^{II} E_\omega - E_v\right). \quad [31]$$

Here, the coefficient

$$B^{II} := -\frac{\partial \ln H^*}{\partial \ln v} = -\frac{\partial \ln \Theta}{\partial \ln v} \quad [32]$$

can be obtained from the distance of adjacent isolines along a line parallel to the v-axis of from the function $\Theta = \Theta(v)$, and the coefficient

$$A_\omega^{II} := \frac{d \ln v}{d \ln \omega} \quad [33]$$

from the displacement of the isolines in horizontal direction on varying the parameter ω. The parameters a and ξ do not appear because the concentration Θ is neither influenced by the rate of the particle exchange at the margins (6) nor by passage events.

4. RESULTS AND DISCUSSION

Now we possess the means to investigate quantitatively the influence of the individual types of interactions contained in our model, i.e.,

- the *marginal barrier*, determining the rate of particle exchange between the marginal sites and the surrounding gas phase (parameter a);
- the additional *attraction* between neighbouring particles (parameter ω); and
- the possibility of *passages*, where—in deviation from the situation in a strict single-file system—neighbouring particles exchange their positions (parameter ξ)

on the temperature dependence of the conversion.

In the example considered so far, the case $E_{H^*} > 0$ only occurred in region III. As will be justified in Section 4.5, the systematic quantitative consideration can indeed be limited to this region. As already indicated in Fig. 8, this region III is characterized by two conditions:

- The channel is *almost completely occupied*. This means that the concentration of vacancies is very low, $(1 - \Theta) \ll 1$ (cf. Fig. 6); i.e., there is most probably not more than one isolated vacancy within the channel. Thus, the particle transport proceeds according to the "vacancy mechanism" considered in (11), where any hop of the particles corresponds to the movement of a vacancy through the entire channel. This implies that, roughly speaking, the time scale of the system behaviour is inversely proportional to the vacancy concentration $(1 - \Theta)$.
- The total conversion is *transport-controlled*. Since with increasing intrinsic conversion rate k the relative dominance of the transport increases, the effectiveness factor decreases, so that $\partial\eta/\partial k < 0$.

4.1. The Simple Case

The situation considered in Fig. 4, which served as an example for Section 3.1, corresponds to the most simple case: there is no hindrance of the exchange at the margins (large a), no attraction of the particles ($\omega = 1$), and passages are excluded completely ($\xi = 0$). Let us consider this case again, this time using the mathematical means of Section 3.2. The quantities necessary to calculate E_{H^*} via Eq. [29] can be obtained as follows. The parameters a and ω were assumed to be constant; i.e., their activation energies E_a and E_ω are set to zero. Moreover, we assumed $\xi = \hat{\xi} \equiv 0$ which implies $A_{\hat{\xi}} = 0$. In region III of Fig. 4, the direction of the isolines gives $A_v = 1$. The value of the coefficient B could be read from the distance between the isolines or from the slope in Fig. 7. The somewhat distorted curves in Fig. 7, however, indicate that this particular piece of information suffers from inaccuracies which can be attributed to the small number of sites, $N = 8$ (which had to be chosen because of numerical problems; cf. the Appendix) (7). Nevertheless, Fig. 7 reveals that the slope of the curves $\eta = \eta(\kappa)$ is nearly independent of v (in this log–log plot, the curves are simply translated along the abscissa). (Reference (7) gives further details supporting this point of view.) Particularly, this implies that B can be calculated from the slope at very large v, even though we are in the region of small v. The case of large v, in turn, coincides with normal (Fickian) diffusion because it corresponds to a very low concentration so that each particle is essentially not influenced by neighbours. Thus, we can calculate the coefficient B via Eq. [24] from the well-known expression

$$\eta = \frac{\tanh \Phi}{\Phi} \quad \text{with the Thiele modulus } \Phi \propto \sqrt{k} \quad [34]$$

(curve ——— in Fig. 9) of normal one-dimensional diffusion, leading in the transport-controlled regime (large k) to the slope

$$\frac{\partial \ln \eta}{\partial \ln k} = -\frac{1}{2}. \quad [35]$$

Inserting all this into Eq. [29] gives for the present case

$$E_{H^*} = \frac{E_{true}}{E_\kappa} \frac{E_v - E_\kappa}{2}. \quad [36]$$

Thus, E_{H^*} is positive if $E_\kappa < E_v$ (as in example - · - · - of Fig. 4) while it is negative if $E_\kappa > E_v$ (as in example - - -). Translated to the "original" activation energies, Eq. [36] reads

$$E_{H^*} = \frac{1}{2} E_{true} \frac{E_M - E_{true} + E_B}{E_{true} - E_B}. \quad [37]$$

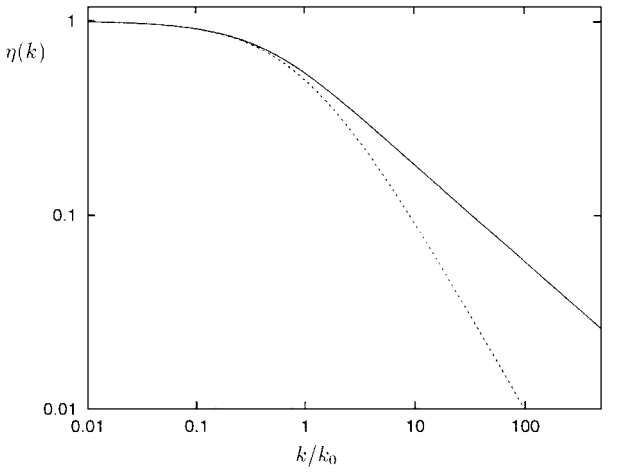

FIG. 9. Dependence of the effectiveness factor η on the scaled intrinsic rate k/k_0 of the conversion for one-dimensional normal diffusion according to Eq. [34] (curve ———) and for a barrier-controlled system according to Eq. [38] (curve - - -).

Since one may assume $E_{\text{true}} > E_{\text{B}}$, the case $E_{\text{H}^*} > 0$ ($E_{\text{app}} > E_{\text{true}}$) occurs if $E_{\text{M}} + E_{\text{B}} > E_{\text{true}}$, i.e., if the sum of the sorption heat and the activation energy of the intracrystalline diffusion exceeds the intrinsic activation energy of the reaction.

4.2. The Influence of the Marginal Barrier

Figure 10 shows the isoline diagram if the particle exchange rate at the margins is decreased (small parameter a). The spacing between the isolines in region III is narrower than in the simple case, indicating that the steepness and thus the coefficient B have increased. In accordance to this, we calculate, analogously to the previous case, the coefficient B from the well-known function $\eta = \eta(k)$ of the barrier-limited case,

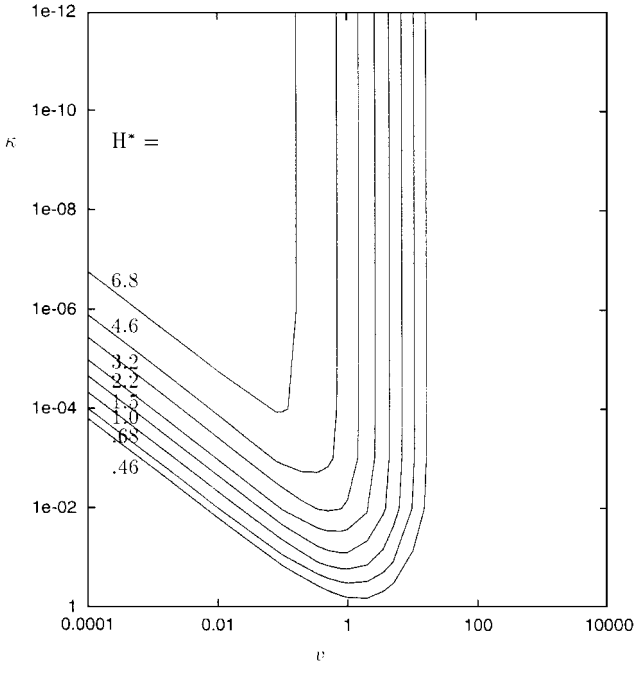

FIG. 10. Isoline diagram of H* for the case of a reduced particle exchange between channel and surrounding ($a = 0.5$), no attractive particle–particle interaction ($\omega = 1$), and a strict single-file condition ($\xi = 0$).

$$\eta = \frac{1}{1 + k\tau_{\text{intra}}} \qquad [38]$$

(curve - - - in Fig. 9) with the slope

$$\frac{\partial \ln \eta}{\partial \ln k} = -1. \qquad [39]$$

The direction of the isolines, however, is identical to Fig. 4, whence the angular coefficient again reads $A_\upsilon = 1$. Therefore,

$$E_{\text{H}^*} = \frac{E_{\text{true}}}{E_\kappa}(E_\upsilon - E_\kappa) = E_{\text{true}}\frac{E_{\text{M}} - E_{\text{true}} + E_{\text{B}}}{E_{\text{true}} - E_{\text{B}}}. \qquad [40]$$

Obviously, the condition $E_{\text{H}^*} > 0$ is fulfilled for the same relation between the activation energies E_κ and E_υ as in the "simple case" as considered in Section 4.1. Only the absolute value of E_{H^*} has increased.

4.3. The Influence of the Attraction

In Fig. 11, the parameter ω is reduced to 10^{-4}, corresponding to a rather strong attraction between neighbouring particles. The borders between the four regions of the (κ, υ)-plane have considerably shifted, so that regions I and II are even outside the diagram. In the upper part of region III, the direction of the isolines now differs from that in Figs. 4 and 10, indicating an angular coefficient of $A_\upsilon \approx 2$. Thus,

$$E_{\text{H}^*} \propto 2E_\upsilon - E_\kappa = 2E_{\text{M}} - E_{\text{true}} + E_{\text{B}}. \qquad [41]$$

This is, in contrast to Eq. [37] or Eq. [40], already positive if $2E_{\text{M}} + E_{\text{B}} > E_{\text{true}}$.

4.4. The Influence of the Passages

So far, we considered the system behaviour at different values of the parameters a and ω, but we always assumed that these parameters themselves do not vary with temperature. This is reasonable because the activation energies of these parameters (E_a and E_ω, respectively) are, for single-file zeolites, mainly much smaller than E_κ and E_υ, as was seen in Section 2.2. Another situation, however, arises if passages are considered because one may assume that the activation energy of this process, E_{X}, even exceeds the marginal potential step, E_{M}. According to the calculation in Section 3.2, we have to compare several isoline diagrams corresponding to different values of the exchange probability ξ. This is done in Fig. 12. If the temperature is increased, one not only moves on the temperature line, but

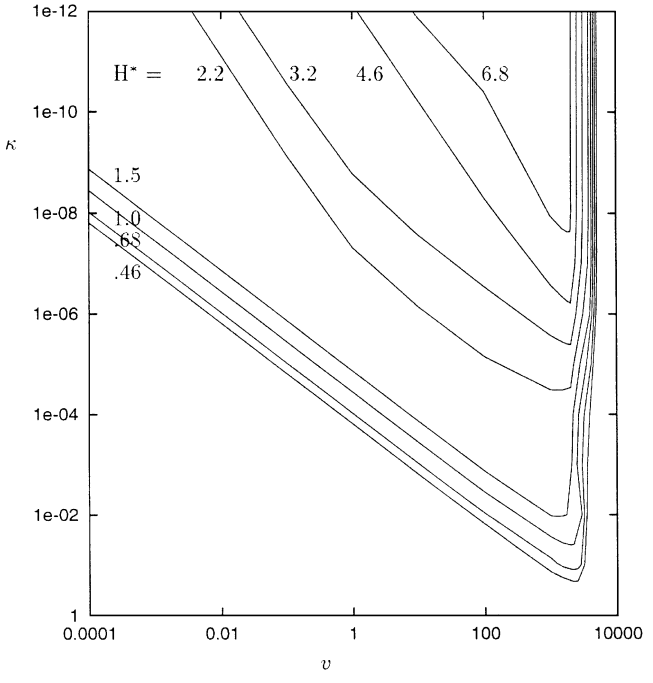

FIG. 11. Isoline diagram of H* for the case of a reduced particle exchange between channel and surrounding ($a = 0.5$), a strong attractive interaction between molecules at adjacent sites ($\omega = 10^{-4}$), and a strict single-file condition ($\xi = 0$).

additionally one has to step from one isoline diagram to the next one according to the increasing parameter ξ.

One observes that in each of the diagrams region III is divided into two subregions (region IIIa to the left and region IIIb to the right, where the separating value of v depends on the order of ξ):

- If the parameter v is large enough (region IIIb), the isolines coincide with those from Fig. 4 ($\xi = 0$, given as dotted lines), whence Eq. [37] is still valid.
- On the contrary, at very small values of v (region IIIa) the isolines become parallel to the v-axis, which implies $A_v = 0$. This means that the parameter v loses its influence on the system dynamics. The physical reason is that the probability of finding a vacancy within the channel has become very small, so that the "vacancy mechanism" becomes negligible and the passages are the only remaining transport mechanism. The time scale of the transport is now determined by the rate of the exchanges, $\xi\Gamma$. In accordance to this, one reads, via Eq. [28], $A_\xi = 1$ from the displacement of the isolines between the diagrams of Fig. 12 (if ξ is increased by a factor of 10^2, the κ-coordinate of the isolines increases by the same factor). Since B (spacing between the isolines) is identical to that of the simple case, Fig. 4, Eq. [29] gives

$$E_{H^*} = \frac{E_{true}}{E_\kappa}\frac{E_\xi - E_\kappa}{2} = \frac{1}{2}E_{true}\frac{E_X - E_{true}}{E_{true} - E_B}. \qquad [42]$$

The condition $E_{H^*} > 0$ is now equivalent to $E_X > E_{true}$.

- In the transition range between region IIIa and IIIb, both ξ and v have influence on H*, but the respective strength of the influence is reduced. As was checked explicitly, the value of E_{H^*} lies between the values of Eqs. [36] and [42] rather than combining to a value of $(E_v + E_\xi - E_\kappa)/2$ which would be higher than in either of the two equations.

Remark. The case $\xi = 1$ in Fig. 12 corresponds to a system with noninteracting particles because passages of the particles are in no way restricted. This can be considered as an idealization of normal diffusion (although there is, of course, a dependence on the coverage and thus on the parameter v even in zeolites with a three-dimensional pore structure, where no single-file behaviour occurs). In contrast to the single-file system considered so far, $\xi = 1$ is then a constant, whence $A_\xi = 0$. Thus, Eq. [42] becomes $E_{H^*} = -E_{true}/2$. This leasds, via Eq. [20], to $E_{app} = E_{true}/2$, which is in complete accordance to the well-known situation in Fickian diffusion-reaction systems.

4.5. Comparison of the Regions

So far, we only considered region III. The question remains whether the situation "$E_{app} > E_{true}$" ("$E_{H^*} > 0$") can be found in one of the other regions as well.

- As mentioned in Section 3.2, $E^{I}_{H^*} = 0$ is region I. This means that apparent and true activation energies are equal, $E_{app} = E_{true}$.
- In region II, one has, according to Eq. [32], $B^{II} > 0$. If one compares Figs. 10 and 11 which differ exclusively in the value of ω, one sees that $A^{II}_\omega < 0$ because in the case of the larger ω (Fig. 10) the isolines of region II are located at smaller values of v than in the case of smaller ω (Fig. 11). This implies via Eq. [31] that $E^{II}_{H^*} < 0$ throughout region II; i.e., in this parameter region the apparent activation energy is surely smaller than the true one, $E_{app} < E_{true}$.
- In region IV, the direction, the mutual distance, and the displacements of the isolines lie between those of its neighbour regions II and III. This implies that also E_{H^*} will be found between the values of these regions. Since $E^{II}_{H^*} < 0$, the value of E_{H^*} in region IV is therefore always smaller than in region III. In most cases, it will be negative as is indicated by the direction of the isolines.

The situation is summarized in Table 1. Thus, the interesting situation $E_{H^*} > 0$ can only be expected to occur in region III.

Remark. As a by-product of this consideration beyond the scope of this paper, one obtains the result that in the chemically controlled regime (i.e., in regions I and II, where transport limitations are negligible because $\eta = 1$) one has $E_{app} = E_{true}$ at lower temperatures and $E_{app} < E_{true}$ at higher temperatures, because on increasing the temperature one will proceed from region I to region II. The same result was recently obtained by a microkinetics simulation for hydroisomerization catalysed by Pt-mordenite (13). This is clearly

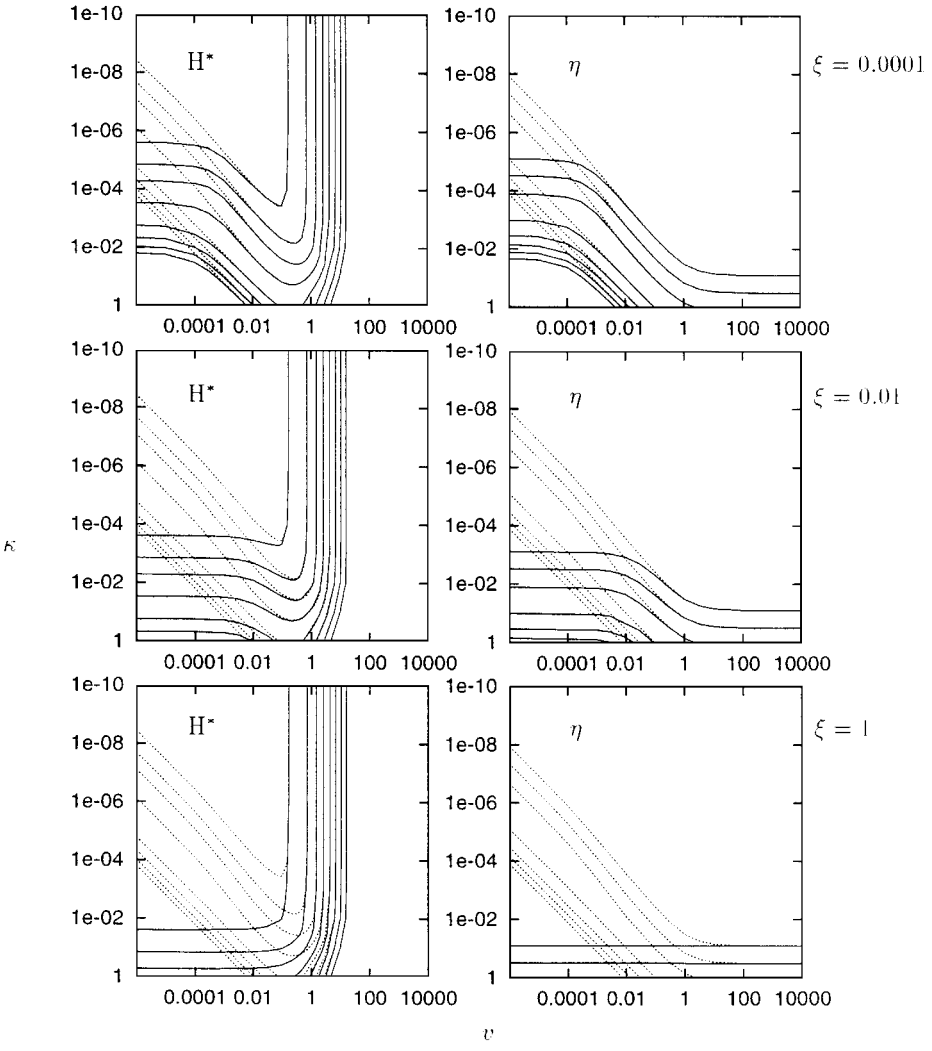

FIG. 12. Isoline diagrams of H* and η for the case of a rapid particle exchange between channel and surrounding ($a = 50$), no attractive particle–particle interaction ($\omega = 1$), and different rates of site exchanges between adjacent molecules which violate the strict single-file condition (different values of ξ). For comparison, the dotted isolines indicate the case of the ideal single-file system without passages ($\xi = 0$) as given in Fig. 4.

TABLE 1

Possible Relations between the Apparent Activation Energy E_{app} and the True Activation Energy E_{app} in a Transport-Reaction System

	Occupation near saturation ($\Theta \approx 1$)	Occupation off saturation ($\partial\Theta/\partial v < 0$)
Chemical control ($\eta \approx 1$)	$E_{app} = E_{true}$	$E_{app} < E_{true}$
Transport control ($\partial\eta/\partial\kappa < 0$)	Both $E_{app} \leq E_{true}$ and $\boldsymbol{E_{app} > E_{true}}$ are possible	$E_{app} < E_{true}$

Note. The four slots of the table correspond to the four parameter regions shown in Fig. 8.

not in contrast to the possible occurrence of the case $E_{app} > E_{true}$ as considered in Refs. (1–3, 5). Such an apparent activation energy larger than the true one was shown to imply transport control while Ref. (13) explicitly refers to the chemically controlled regime where—according to the results just presented—this case $E_{app} > E_{true}$ is excluded.

CONCLUSION

The isoline diagram proves to be a very useful tool to investigate systematically the temperature behaviour of transport-reaction systems. It was applied to systems where the transport follows the pattern of single-file diffusion (the particles are forced to maintain their order). The model was generalized by the introduction of

$$
\begin{aligned}
0 = &- \underbrace{k}_{\text{conversion}} \eta_i^{\cdots} \\
&- \Big(\underbrace{\alpha(1-\sigma_1)}_{\text{adsorption left}} + \underbrace{\varepsilon\sigma_1(1-\Omega\sigma_2)}_{\text{desorption left}} \Big) \eta_i^{\cdots} \\
&- \sum_{j=1}^{N-1} \Big(\underbrace{\Gamma(1-\Omega\sigma_{j-1})\sigma_j(1-\sigma_{j+1})}_{\text{hop } j \to j+1} + \underbrace{\Gamma(1-\sigma_j)\sigma_{j+1}(1-\Omega\sigma_{j+2})}_{\text{hop } j \leftarrow j+1} \Big) \eta_i^{\cdots} \\
&- \Big(\underbrace{\varepsilon(1-\Omega\sigma_{N-1})\sigma_N}_{\text{desorption right}} + \underbrace{\alpha(1-\sigma_N)}_{\text{adsorption right}} \Big) \eta_i^{\cdots} \\
&+ \Big(\underbrace{\alpha\sigma_1}_{\text{succeeded adsorption left}} + \underbrace{\varepsilon(1-\sigma_1)(1-\Omega\sigma_2)}_{\text{succeeded desorption left}} \Big) \begin{cases} \Theta^{0\sigma_2\cdots\sigma_N}, i = 1 \\ \eta_i^{(1-\sigma_1)\cdots}, \text{else} \end{cases} \\
&+ \sum_{j=1}^{N-1} \Big(\underbrace{\Gamma(1-\Omega\sigma_{j-1})(1-\sigma_j)\sigma_{j+1}}_{\text{succeeded hop } j \to j+1} + \underbrace{\Gamma\sigma_j(1-\sigma_{j+1})(1-\Omega\sigma_{j+2})}_{\text{succeeded hop } j \leftarrow j+1} \Big) \begin{cases} \eta_{i+1}^{\cdots\sigma_{i-1}0*\sigma_{i+2}\cdots}, i = j \\ \eta_{i-1}^{\cdots\sigma_{i-2}*0\sigma_{i+1}\cdots}, i = j+1 \\ \eta_i^{\cdots\sigma_{j+1}\sigma_j\cdots}, \text{else} \end{cases} \\
&+ \Big(\underbrace{\varepsilon(1-\Omega\sigma_{N-1})(1-\sigma_N)}_{\text{succeeded desorption right}} + \underbrace{\alpha\sigma_N}_{\text{succeeded adsorption right}} \Big) \begin{cases} \Theta^{\sigma_1\cdots\sigma_{N-1}0}, i = N \\ \eta_i^{\cdots(1-\sigma_N)}, \text{else} \end{cases} \\
&- \Big(\underbrace{\zeta\sigma_1}_{\text{passage left}} \Big) \eta_i^{\cdots} \\
&- \sum_{j=1}^{N-1} \Big(\underbrace{\xi\Gamma\sigma_j\sigma_{j+1}}_{\text{passage } j \leftrightarrow j+1} \Big) \eta_i^{\cdots} \\
&- \Big(\underbrace{\zeta\sigma_N}_{\text{passage right}} \Big) \eta_i^{\cdots} \\
&+ \Big(\underbrace{\zeta\sigma_1}_{\text{succeeded passage left}} \Big) \begin{cases} \Theta^{1\sigma_2\cdots\sigma_N}, i = 1 \\ \eta_i^{1\sigma_2\cdots}, \text{else} \end{cases} \\
&+ \sum_{j=1}^{N-1} \Big(\underbrace{\xi\Gamma\sigma_j\sigma_{j+1}}_{\text{succeeded passage } j \leftrightarrow j+1} \Big) \begin{cases} \eta_{i+1}^{\cdots\sigma_{i-1}1*\sigma_{i+2}\cdots}, i = j \\ \eta_{i-1}^{\cdots\sigma_{i-2}*1\sigma_{i+1}\cdots}, i = j+1 \\ \eta_i^{\cdots11\cdots}, \text{else} \end{cases} \\
&+ \Big(\underbrace{\zeta\sigma_N}_{\text{succeeded passage right}} \Big) \begin{cases} \Theta^{\sigma_1\cdots\sigma_{N-1}1}, i = N \\ \eta_i^{\cdots\sigma_{N-1}1}, \text{else} \end{cases}
\end{aligned}
$$

$$\forall \sigma_1, \ldots, \sigma_N = 0, 1; \forall i = 1, \ldots, N.$$

FIG. 13. Set of equations determining the mean number H^* of reactant molecules within the channel in a monomolecular irreversible conversion of the intrinsic rate k. The quantities $\Theta^{\sigma_1\cdots\sigma_N}$ denote the probabilities of the configurations $(\sigma_1, \ldots, \sigma_N)$ of the system, where σ_i tells whether site i is occupied or not. These quantities are determined by detailed balance. The unknown variables of the set, $\eta^{\sigma_1\cdots\sigma_{i-1}*\sigma_{i+1}\cdots\sigma_N}$, represent the probabilities of the configurations $(\sigma_1, \ldots, \sigma_{i-1}, 1, \sigma_{i+1}, \ldots, \sigma_N)$, where site i is occupied by a reactant molecule. Each equation of the set corresponds to one of these configurations, were the underbraced coefficients give the rates of the transitions which lead out of or into the considered configuration. The physical processes causing these transitions are indicated by the respective labels. The output quantity, H^*, is simply the sum over all the unknown variables. For a detailed derivation see (6).

• surface barriers, determining the rate of particle exchange between the marginal sites and the surrounding gas phase,

• an additional attractive interaction of adjacent molecules,

• and a certain possibility of mutual passages of the molecules, exchanging—deviating from the ideal single-file system—the positions of these particles.

It turned out that for this model, in striking contrast to systems undergoing normal diffusion, the apparent activation energy E_{app} of the total conversion can exceed the intrinsic activation energy E_{true}. The difference E_{H^*} between both activation energies is dependent on the chosen parameters of the model given by Eqs. [37], [40], [41], and [42], respectively. These equations relate this difference to the activation energies of the involved microdynamic processes. A positive difference E_{H^*} is possible to occur if

• the channel is almost completely occupied ($1 - \Theta \ll 1$) and

• the total conversion is transport controlled ($\partial\eta/\partial k < 0$)

(referred to as parameter region III). Quantitatively, the model leads to the following behaviour. In a strict single-file system where passages are excluded completely, a positive energy difference E_{H^*} is possible only if the sorption heat is larger than the intrinsic activation energy of the conversion (or, if there is a strong attraction between the molecules, larger than roughly half the intrinsic activation energy). If, however, there is a certain possibility that neighbouring particles can exchange their positions, the case $E_{\mathrm{app}} > E_{\mathrm{true}}$ can occur if the activation energy of these passages exceeds the intrinsic activation energy of the conversion. Estimated activation energies as given in Section 2.2 indicate that the case $E_{\mathrm{app}} > E_{\mathrm{true}}$ ($E_{\mathrm{H}^*} > 0$) is well in the range of realistic conditions.

APPENDIX A

The numerical procedure which was used for this paper is described in (6), where the interested reader may find a detailed derivation. It yields the mean number H^* of reactant molecules and the mean occupancy Θ (output quantities) dependent on the parameters (input quantities) v, a, ω, ξ, κ, and N. Its essence is a rather huge set of linear equations which can be solved numerically. Since the set of equations had to be generalized in order to account for the passage not yet considered in (6), Fig. 13 shows the set used for this paper.

By the way, the algorithm is equally able to yield the mean intracrystalline lifetime τ_{intra}, the residence time distribution $\varphi(\tau)$, and all its moments. Moreover, one gets all the quantities locally at the individual sites as well, i.e., their profiles along the channel, such as the total concentration profile or the concentration profile of the reactant molecules. The drawback of the algorithm is the immense size of the set of equations, which limits, due to computer memory size, the maximal channel length N to be investigated. Here, as in (6), we have chosen $N = 8$, which, however, proves sufficient to assess the principal behaviour of the considered systems.

APPENDIX B: SYMBOLS

A_v	Angular coefficient of the isolines
A_a, A_ω, A_ξ	Displacement coefficients
a	Dimensionless parameter, defined by Eq. [9]
B	Slope coefficient of the isoline diagram
D	Single-particle diffusion coefficient
$E_{(\cdot)}$	Activation energy of the quantity $(\cdot)$
E_{app}	Apparent activation energy of the conversion
E_{true}	True activation energy of the conversion
E_{B}	Potential barrier between adjacent sites
E_{I}	Interaction energy
E_{M}	Potential barrier at the margins (sorption heat)
E_{X}	Potential barrier for mutual passages of molecules at adjacent sites
K	Total output rate of product molecules
k	Intrinsic conversion rate
l	Distance between adjacent sites
N	Number of sites per channel
v	Dimensionless parameter, defined by Eq. [8]
α	Adsorption rate of the isolated particle
Γ	Jump rate of the isolated particle
ε	Desorption rate
H^*	Mean number of reactant molecules within the channel
η	Effectiveness factor
Θ	Coverage (relative concentration, occupation)
κ	Dimensionless parameter, defined by Eq. [10]
ξ	Relative rate of passages
τ_{intra}	Mean intracrystalline life time
Φ	Thiele modulus
ω	Parameter of the attractive interaction

ACKNOWLEDGMENTS

We thank Professor W. M. H. Sachtler for stimulating discussions. We are obliged to the Studienstiftung des Deutschen Volkes and to the Deutsche Forschungsgemeinschaft (SFB 294) for financial support of this work.

REFERENCES

1. Lei, G.-D., and Sachtler, W. M. H., *J. Catal.* **140**, 601 (1993).
2. Karpiński, Z., Ghandi, S. N., and Sachtler, W. M. H., *J. Catal.* **141**, 337 (1993).
3. Lei, G. D., Carvill, B. T., and Sachtler, W. M. H., *Appl. Catal.* **142**, 347 (1996).

4. Kärger, J., Petzold, M., Pfeifer, H., Ernst, S., and Weitkamp, J., *J. Catal.* **136**, 283 (1992).
5. Rödenbeck, C., Kärger, J., and Hahn, K., *J. Catal.* **157**, 656 (1995).
6. Rödenbeck, C., Kärger, J., and Hahn, K., *Phys. Rev. E* **55**, 5697 (1997).
7. Rödenbeck, C., thesis, University of Leipzig, Faculty of Physics and Geosciences, submitted.
8. Kukla, V., Kornatowski, J., Demuth, D., Girnus, I., Pfeifer, H., Rees, L., Schunk, S., Unger, K., and Kärger, J., *Science* **272**, 702 (1996).
9. Hahn, K., Kärger, J., and Kukla, V., *Phys. Rev. Lett.* **76**, 2762 (1996).
10. Landau, L. D., and Lifschitz, E. M., "Lehrbuch der Theoretischen Physik," Vol. 5. Akademie-Verlag, Berlin, 1987.
11. Rickert, H., *Z. Phys. Chem. NF* **43**, 129 (1964).
12. Keffer, D., McCormick, A. V., and Davis, H. T., *Mol. Phys.* **87**, 367 (1996).
13. Van de Runstraat, A., Van Grondelle, J., and Van Santen, R. A., *J. Catal.* **167**, 460 (1997).